Journal of the European Ceramic Society 17 (1997) 1523–1532

PII: S0955-2219(96)00247-6
0955-2219/97/$17.00

Elastic Properties of Ceramic Oxides Used in Solid Oxide Fuel Cells (SOFC)

A. Selçuk & A. Atkinson

Imperial College of Science, Technology and Medicine, Department of Materials, Prince Consort Road, London SW7 2BP UK

(Received 16 August 1996; revised version received 21 November 1996; accepted 25 November 1996)

Abstract

Measurements are presented for the effective Young's (E) and shear (G*) moduli and Poisson's ratio of some materials of interest for solid oxide fuel cells (SOFC), namely 10 and 20 mol% Gd_2O_3 doped CeO_2 (GCO), 3 and 8 mol% Y_2O_3 stabilized ZrO_2 (TZP and YSZ), and 75 mol% NiO-YSZ. The dependence of moduli on porosity was characterized by employing both theoretical (composite sphere method, CSM) and empirical (exponential, nonlinear, and linear) equations. The theoretical and empirical equations were tested by determining the goodness of fit of the equations to the experimental data and the standard error of estimation. All the equations described the modulus-porosity relationships equally well, except that, for NiO-YSZ, the empirical equations yield better fits than the CSM equations. This was attributed to the fact that the CSM equations, derived for two-phase composites, might not hold for calculating the effective moduli of three-phase composites, such as these NiO-YSZ materials. © 1997 Elsevier Science Limited.*

1 Introduction

In the past, nearly all materials research activities on the design and fabrication of solid oxide fuel cells (SOFC) have been devoted to optimizing electrochemical, thermal and microstructural properties. This has resulted in several electrochemically sound SOFC systems. However, comparatively little research has been carried out on the mechanical properties of SOFC components and their impact on the lifetime of SOFC operation. Target SOFC lifetimes are of the order of 10^4 to 10^5 hours. This depends not only on the stability of electrochemical behaviour, but also on the ability of the structure to withstand mechanical stresses arising from operation and residual stresses from the fabrication of the cells.

A fundamental component in planar SOFCs is the integrated PEN structure (PEN = Positive electrode–Electrolyte–Negative electrode), which is produced by ceramic powder processing. Tape casting is widely used to produce the dense electrolyte to which porous electrodes are added by screen printing. Alternatively, the individual layers of PEN components can be joined together in green ceramic form by tape calendaring in a continuous process and then co-sintered.[1] The mechanical properties of the individual layers in the integrated PEN structure structure will depend on the defects and impurities introduced during processing; for example it is well established that the Young's modulus (E) of ceramic materials changes with porosity and impurity content. Since three individual layers of different ceramic components are joined together in PENs, the overall reliability of the PEN structures will be governed not only by the properties of the individual layers, but also by those of the interfaces between them. Residual stresses will arise from the difference between the thermal expansion coefficients (α) and the effective Young's modulus (E^*) of adjacent layers.[2] These mismatch stresses can result in the delamination of layers or the formation of microcracks in the weaker layer.

The compatibility of the thermal expansion coefficients of SOFC components is one of the design criteria, and the relevant data for most of the prospective components are available in the literature. On the other hand, the reported data on the elastic properties of the SOFC components are limited to the electrolyte material, yttria-stabilized zirconia (YSZ). Scafe *et al.* recently reported the porosity dependence of Young's modulus of tape-cast YSZ containing 8 mol% yttria, determined by the ultrasonic 'pulse-echo' technique. The elastic constants of single-crystal and polycrystalline samples of yttria-stabilized zirconia with an yttria content in the range 2 to 17 mol% have also been reported in the literature.[4–6] The elastic constants

Table 1. Properties of the fabricated samples

Material code	*Composition condition*	*Sintering (μm)*	*Thickness (mm)*	*Diameter density (%)*	*Relative structure*	*Crystal*
10GCO	$Ce_{0.9}Gd_{0.1}O_{1.95}$	1500°C, 1 h	190–205	21	95–98	Cubic
20GCO	$Ce_{0.8}Gd_{0.2}O_{1.90}$	1500°C, 1 h	200–215	21	94–98	Cubic
YSZ	8mol%Y_2O_3–ZrO_2	1300°C, 3 h	175–190	21	93–99	Cubic
NiO-YSZ	75 mol% NiO–YSZ	1300°C, 2 h	515–550	21	86–92	Cubic
TZP	3mol%Y_2O_3–ZrO_2	1500°C, 1 h	165–175	22	90–95	Tetragonal

of both single-crystal and polycrystalline materials have been obtained from bulk samples, most of which were produced by completely different processing methods from those commonly employed for fabrication of SOFC electrolytes. Hence, the reported data may not be reliable for use in SOFC modelling and material design studies.

This work reports a study of the porosity dependence of Young's and shear moduli and Poisson's ratio of typical SOFC materials, namely 10 and 20 mol% Gd_2O_3 doped CeO_2 (low-temperature electrolyte), NiO-YSZ two-phase mixture (precursor for composite anode), tetragonal zirconia polycrystal (TZP), and 8 mol% Y_2O_3 stabilized zirconia (YSZ) (electrolytes). Moreover, these materials have been studied in forms that are representative of their use as components in the fuel cells.

2 Experimental Procedure

The general characteristics of the samples studied in the present work are given in Table 1. The samples were produced in the form of circular discs by a polymer vehicle ceramic fabrication process, in which for each material a viscous ceramic powder-binder mixture was prepared and then shaped into a green tape by extrusion. Circular discs were cut from the green tapes, and, after binder burnout at 400°C, densified by sintering in air at the temperatures given in Table 1. For NiO-YSZ and YSZ compositions, additional disc samples were prepared by cold compacting powders and sintering the compacts at 1350°C and 1500°C, respectively. The final density of these samples was above 98% of theoretical. Both faces of these samples were ground to obtain an even thickness of approximately 500 μm, and then heated to sintering temperatures for the relaxation of residual stresses induced by grinding.

The density of samples was determined by the geometrical method. The diameter of each sample was measured using digital calipers (Mitutoyo, resolution 10 μm); six readings were taken at 30° intervals covering the full rotation of the sample. The thickness of each sample was measured using a digital micrometer (Mitutoyo, resolution 1 μm) with round probe-tips, enabling the measurements to be made between two point contacts at opposite sides of the sample. In order to minimize the effect of thickness variation on the accuracy of measurements, ten measurements were taken at certain locations, namely one measurement at the centre of symmetry and three and six measurements on the circles at about 1/3 and 3/4 of the radius of the sample, respectively. The volume of each sample was determined using the average values of thickness and diameter. The range of measured geometrical densities for each set of samples is given in Table 1.

The elastic properties of samples, namely effective Young's and shear moduli, E^* and G^*, and Poisson's ratio, ν^*, were determined by the impulse excitation technique (IET) using a commercially available apparatus (GrindoSonic MK5 'Industrial', J. W. Lemmens, Belgium). The procedure of the IET tests was that a circular disc sample was supported by a foam material on its nodal lines, and then excited by a light mechanical impulse. The nodal lines of the sample in flexural and torsional resonance modes are illustrated in Fig. 1 (a). The mechanical impulse was applied to the sample by dropping a steel ball, with a diameter of 0·5 mm, at certain locations on the sample, which produced the flexural and torsional resonance (Fig. 1 (b)). A microphone, located beneath the sample, was used to transmit the sound waves to the signal processing unit, and the fundamental resonance frequencies in both flexural and torsional modes were identified. The values of E^* and G^* for each sample were computed according to the equation[7]

$$M^* = \rho D^4(1 - \nu^2)(\pi f_{mn}/t\lambda_{mn}) \quad (1)$$

where M^* is E^* or G^*, λ_{mn}, is a constant dependent on the Poisson's ratio (ν) and the geometry of the sample, f_{mn} is the resonance frequency, D the diameter, t the thickness, and ρ the density of the sample. The subscripts m and n are characteristic of the vibration mode. For the torsional fundamental mode, $m = 2$ and $n = 0$, and for the

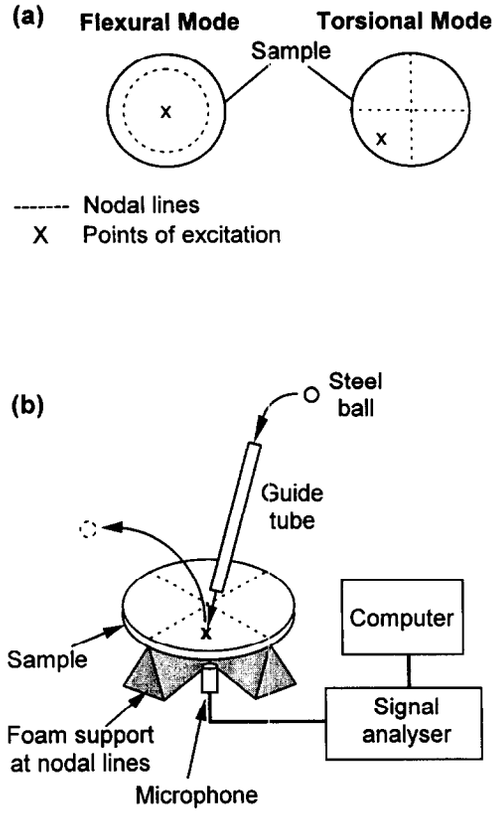

Fig. 1. A schematic illustration of (a) the fundamental flexural- and torsional-mode nodal lines and the points of excitation on disc samples, and (b) the setup for the operation of the impulse excitation technique (IET) in torsional mode.

flexural fundamental mode $m = 0$ and $n = 1$. The values of ν^* were also computed according to a formulation expressed in a simplified form by

$$\nu^* = g\{(f_{20}/f_{01}), (2t/D)\} \quad (2)$$

where g is a numerical function.[7]

3 Effective Moduli

Many investigators have analysed the effective elastic moduli of porous solids by treating them as two-phase materials, with the second phase being a void, and several empirical equations have been derived for describing the effective elastic moduli as a function of porosity. Also, some theoretical expressions have been obtained from more fundamental analytical models, which encompass the effect of the shape, volume, distribution and interaction of pores on the elastic constants. In the present work, three empirical equations and one theoretical equation were investigated to describe the relationship between the measured elastic constants and porosity of the SOFC materials.

3.1 Empirical relations

The three empirical relations expressing the effective moduli as a function of porosity, which were employed to fit the experimental modulus-porosity data, are given by the equations

$$M^* = M_o(1 - b_M p) \quad (3)$$

$$M^* = M_o \exp(- b_M P) \quad (4)$$

$$M^* = M_o \left[1 - \frac{b_M p}{1 + (b_M - 1)p}\right] \quad (5)$$

where M^* is the modulus, E^* or G^*, at the fractional porosity, p ($0 \leq p \leq 1$), b_M is an empirical constant defining the porosity dependence of M^*, and M_o is the modulus, E_o or G_o of a sample with zero porosity. These equations may be considered as semi-empirical since they have some theoretical support. Dean and Lopez[8] have summarized the background theory and relative merits of the empirical relations used in practice, including all the three equations employed in this work.

The linear relation, eqn (3), was first used to analyse modulus-porosity data from polycrystalline BeO by Fryxell and Chandler.[9] It assumes a linear relationship between the elastic moduli and porosity of a solid. The exponential relation, eqn (4), which was proposed by Spriggs,[10] has found wide use in fitting modulus-porosity data for ceramics. The non-linear relation eqn (5), was proposed by Hasselman[11] for the moduli of materials with dilute distributions of spherical pores. Both the exponential and non-linear relations, eqns (4) and (5), are based on the treatment of porous solids as two-phase materials with one phase being spherical pores distributed randomly in the matrix.

3.2 Theoretical relations

There have been several theoretical treatments of two-phase composites[12–14] with each phase having a different elastic modulus. But the analytical procedures available for treating two-phase solids as continuum materials are not directly applicable where the second phase is a void. However, Ramakrishnan and Arunachalam[15,16] recently developed a theoretical approach for determining the effective moduli of porous solids with randomly distributed pores on the basis of the composite sphere method (CSM). This method, which was first introduced by Hashin,[12,13] models a two-phase material as a sphere of the matrix material with a spherical pore concentrically placed in it, and approximates the real geometry of the two-phase material as an assembly of such composite spheres of different sizes. According to the results from the model calculations of Ramakrishnan and Arunachalam,[15,16] the effective Young's and shear moduli, E^* and G^*, and the effective Poisson's ratio, ν^* are described as a function of porosity by the equations

$$E^* = E_o(1-p)^2/(1+b_E p) \quad (6)$$

$$G^* = G_o(1-p)^2/(1+b_G p) \quad (7)$$

$$\nu^* = 0{\cdot}25(4\nu_o + 3p - 7\nu_o p)/(1+2p-3\nu_o p) \quad (8)$$

where ν_o is Poisson's ratio at zero porosity, $b_E = (2 - 3V_o)$ and $b_G = (11 - 19\nu_o)/(4 + 4\nu_o)$. In the present work, these equations along with the empirical ones were employed to describe the porosity dependence of the terms, E^*, G^*, and ν^* for the studied materials.

4 Data Analysis

The empirical relations, namely the linear, exponential, and non-linear equations, given in eqns (3), to (5), were fitted to the experimental modulus versus porosity data from each set of samples, employing computer-aided iterative calculations. The goodness of the fit between each fitted equation and data was determined by calculating the fitting parameter, S

$$S = 1 - \left\{ \sum_{i=1}^{n} (M_{i,\exp} - M_i)^2 \Big/ \sum_{i=1}^{n} (M_{i,\exp} - \overline{M_i})^2 \right\} \quad (9)$$

where $S = 1$ indicates a perfect fit and values of $S > 0{\cdot}8$ are considered as good fits, M_i is the value of modulus (E^* or G^*) calculated from the fitted equation for a given porosity, and $M_{i,\exp}$ and $\overline{M_i}$ are the measured modulus values and the mean value of M_i, respectively. A computer program was run to yield the best fit of the equations to the data under the condition that the best fit is achieved when the value of S is maximized. The adjustable parameters for curve fitting were E_o, G_o, b_E, and b_G (eqns (3)–(5)), which were determined for each material by maximizing the value of S. Poisson's ratio, ν^*, as a function of porosity was then calculated from the expression for Poisson's ratio in isotropic materials

$$\nu^* = \frac{E^*}{2G^*} - 1 \quad (10)$$

In the CSM equations, eqns (6) and (7), the effective Young's modulus, E^*, is related to the effective shear modulus, G^*, according to eqn (10) and the porosity dependence constants, b_E and b_G, are determined by the value of Poisson's ratio at zero porosity, ν_o. That is, for any value of porosity, p, the CSM expressions for E^* eqn (6) and G^* eqn (7)) are interrelated according to eqn (10). The CSM theory predicts the value of G^* once the values of E_0 and ν_o are determined, or vice versa. Hence, the achievement of the best fit between the CSM equations and data required the simultaneous maximization of all the values of S, calculated from the fitted equations, eqns (6)–(8). This was obtained by running the same iterative computation as described for fitting the empirical equations to data. The adjustable parameters used for curve fitting were E_o and ν_o.

The elastic constants, c_{11}, c_{12}, and c_{14}, of the single-crystal tetragonal zirconia and YSZ have been reported in the literature.[4–6] From these constants, theoretical estimates of E_o or G_o for a polycrystalline structure were obtained using the Hashin–Shtrikman bounds for the polycrystalline moduli[14] and the appropriate relationships of linear elastic theory.[17] The procedure for these calculations has been summarized by Ingel and Lewis.[4] The resulting estimates of E_o, G_o, and ν_o for polycrystalline TZP and YSZ were used to assess the accuracy of both empirical and analytical (CSM) equations in describing the modulus-porosity relation of these materials.

The standard errors of the E^*, G^*, and ν^* values, predicted for the experimental data by both the CSM and empirical equations, were determined using the standard error function

$$\sigma_{y-x}\left\{\left[\frac{1}{n(n-2)}\right]\left[n\Sigma y^2 - (\Sigma y)^2 - \frac{n\Sigma xy - (\Sigma x)(\Sigma y)^2}{n\Sigma x^2 - (\Sigma x)^2}\right]\right\}^{1/2} \quad (11)$$

where n is the number of data pairs in a data set, x denotes the experimental values of E^*, G^* or ν^*, and y the predicted ones. This function gives the average of the standard error in the prediction of y for any x in a series. The percentage standard error was obtained by dividing the standard error by the values of E_o, G_o, and ν_o, estimated for zero porosity.

5 Results and Discussion

5.1 Porosity dependence of effective moduli

Figures 2 and 3 show the plots of the effective moduli, E^* and G^*, and Poisson's ratio, ν^*, as a function of porosity for TZP and YSZ samples, respectively. The modulus-porosity relationships, determined using the linear, exponential, non-linear, and CSM relations, are shown by separate lines in Figs 2 and 3. In these plots, the modulus-porosity data, reported in the literature, for single-crystal[4–6] and polycrystalline[3,18,19] samples of TZP and YSZ with similar compositions to our samples, are also shown by different symbols. The literature data were obtained using the ultrasonic 'pulse-echo' technique. The Young's moduli (empty squares in Fig. 3), reported for polycrystalline YSZ by Scafe *et al.*,[3] are the most relevant

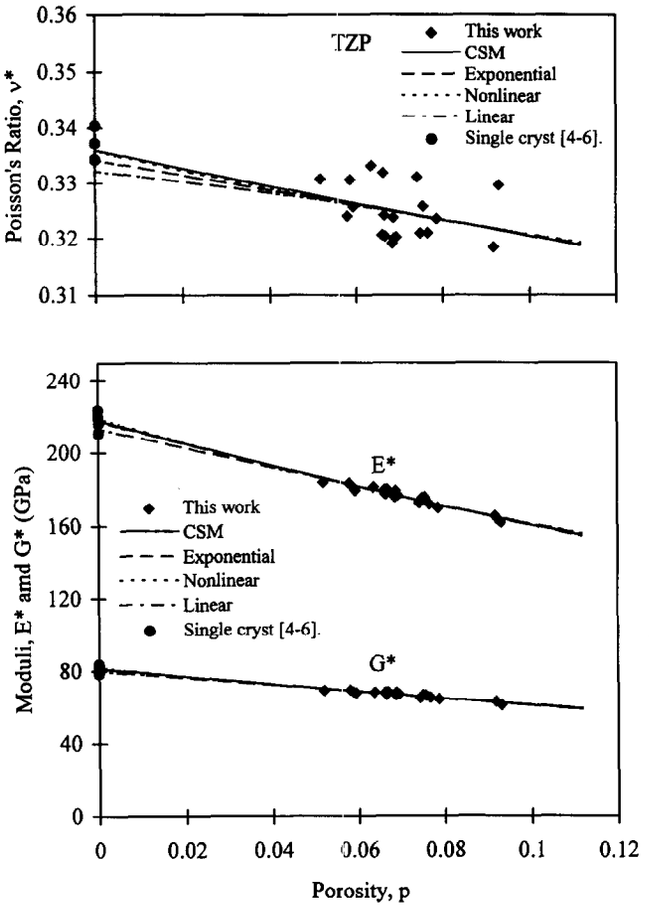

Fig. 2. Variation of Young's (E) and shear (G) moduli and Poisson's ratio (ν) with porosity for TZP samples. The fitted equations and the data from the literature are illustrated by separate lines and symbols, respectively.

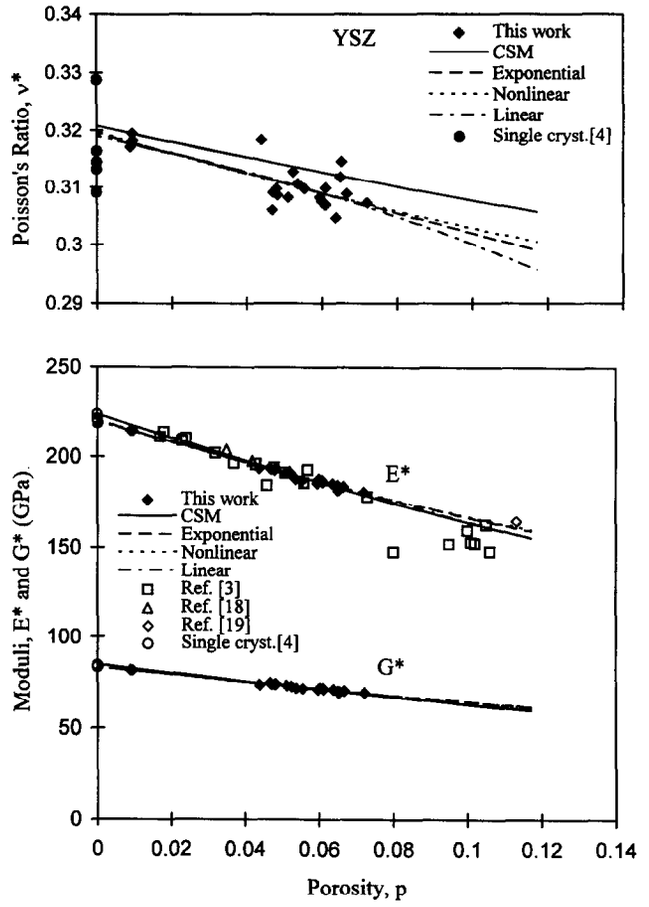

Fig. 3. Young's (E) and shear (G) moduli and Poisson's ratio (ν) as a function of porosity for YSZ samples. The fitted equations and the data from the literature are illustrated by separate lines and symbols, respectively.

data to compare with the present results because those samples were also prepared as thin plates for the SOFC application. As can be seen from Fig. 3, there is good agreement between the present results and the literature data for YSZ.

The zero porosity moduli, E_o and G_o and their porosity dependence constants, b_E and b_G, were calculated using the empirical and theoretical (CSM) equations, fitted to the modulus-porosity data from TZP and YSZ samples. For each sample set, Poisson's ratio at zero porosity, ν_o, was determined from eqn (10). A summary of the best fit zero-porosity constants, E_o, G_o, and ν_o, and the porosity dependence constants, b_E and b_G, is given in Table 2. The estimates of E_o G_o and ν_o, for polycrystalline TZP and YSZ, determined from

Table 2. The best fit values of zero-porosity moduli, E_o and G_o, the porosity dependence constants, b_E and b_G, and Poisson's ratio, ν_o, of TZP and CSZ samples

Material	*Equation*	E_o	G_o	ν_o	b_E	b_G
YSZ	Exponential	220·27	83·47	0·320	−2·76	2·63
	Non-linear	220·47	83·52	0·320	2·84	−2·69
	Linear	219·53	83·22	0·319	−2·50	−2·39
	CSM	223·85	84·74	0·321	1·04	0·93
	From single crystal[a]	220·84 ± 0·8%	83·33 ± 0·5%	0·316 ± 2·3%	—	—
TZP	Exponential	217·46	81·49	0·334	−3·01	2·91
	Non-linear	218·94	81·94	0·336	3·23	−3·09
	Linear	213·19	80·02	0·332	−2·48	−2·41
	CSM	217·78	81·50	0·336	0·99	0·86
	From single crystal[a]	216·17 ± 2·7%	80·83 ± 2·9%	0·337 ± 0·9%	—	—

[a]The average of the polycrystalline estimates of the single-crystal constants, reported in the literature. (Refs 4–6). The standard deviations are given in percentages.

Table 3. Percentage deviation of the fitted moduli, extrapolated to zero porosity, from the estimates derived from single-crystal elastic constants

Material	*Zero porosity moduli*	*Percentage deviation*			
		Exponential	*Non-linear*	*Linear*	*CSM*
TZP	E_o	0·60	1·28	1·38	0·75
	G_o	0·83	1·39	1·00	0·84
YSZ	E_o	0·26	0·17	0·59	1·36
	G_o	0·50	0·43	0·79	1·02
Average % deviation					
TZP	E_o & G_o	0·71	1·33	1·19	0·79
YSZ	E_o & G_o	0·83	0·30	0·69	1·19

Based on Refs 4–6.

the reported elastic constants, c_{11}, c_{12}, and c_{14}, of single crystals, are also included in Table 2 for comparison.

There is good agreement between the values of E_o, G_o, and ν_o from the fitted equations and the polycrystalline estimation using the single crystal moduli.[4–6] The corresponding percentage deviation between both sets of moduli values is mostly below 1%, as shown in Table 3. The values of percentage deviation for the empirical equations (eqns (3) to (5)) are smaller than the standard deviations of the reported single-crystal moduli (Table 2). The CSM equations (eqns (6) and (7)) tend to yield slightly larger values of percentage deviations than the empirical equations.

The plots of the effective moduli, E^* and G^*, and Poisson's ratio, ν^*, as a function of porosity for 10GCO, 20GCO and NiO-YSZ samples, together with the fitted curves from the empirical and CSM equations, are shown in Figs 4, 5, and 6, respectively. The unknown values of the zero-porosity elastic constants, E_o, G_o, and ν_o, and the porosity dependence constants, b_E and b_G, were estimated using both empirical and CSM equations according to the procedure described above. The resulting data from the fitted equations are summarized in Table 4.

The modulus-porosity relations for TZP, 10GCO, 20GCO, and NiO-YSZ samples, presented in Table 4, are the first data made available in the literature. Although Sammes and Zhang[20] reported an average value of Young's modulus, E^* = 147·2 (± 16), GPa, for 20GCO with porosity in the range 7 to 12%, the modulus-porosity relation was not given in their report. They obtained this value of E^* from the results of four-point bending tests at room temperature. Our moduli data for 20GCO are limited to a porosity range from 1·5 to 6%. By extrapolation of our results using the fitted equations in Fig. 5, we estimate a value of E^* = 158–160 GPa for 10% porosity. The difference between the two values of E^* is not significant, being less than one standard deviation of the value measured by Sammes and Zhang. It may also be mentioned that, for use in SOFCs, all the materials studied, except NiO-YSZ, are required to have high densities. Hence the experimental data, comprising up to 30 values of effective moduli, E^* and G^*, were obtained from samples with a porosity, $p < 16\%$ ($0{\cdot}009 < p < 0.16$). This limited range of porosity is expected to reduce the accuracy of estimating the effective moduli for very large values of porosity, using the constants given in Tables 2 and 4.

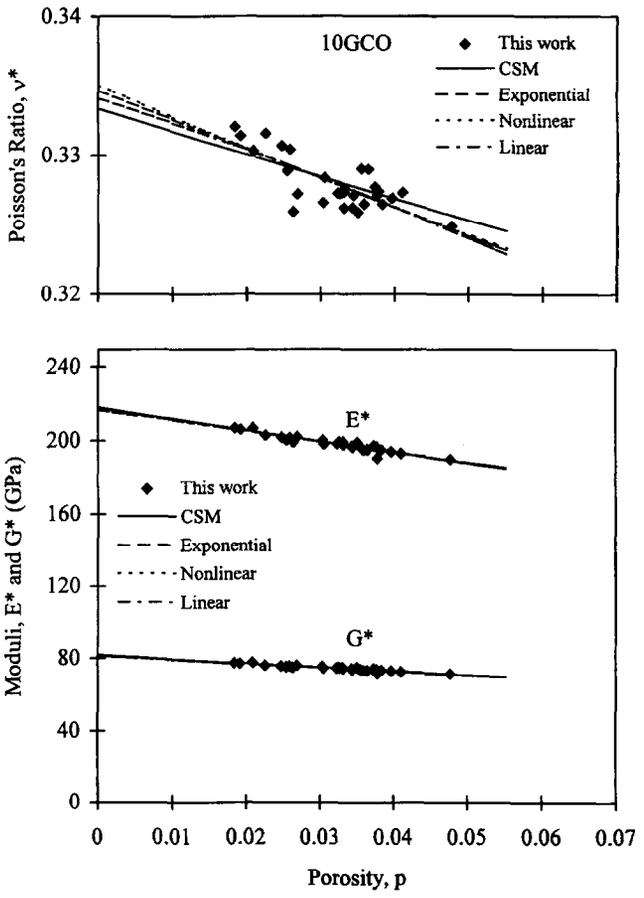

Fig. 4. Effective Young's (E^*) and shear (G^*) moduli and Poisson's ratio (ν^*) as a function of porosity for 10GCO samples. The fitted equations are illustrated by separate lines, as shown in the legend.

Table 4. Best fit values of zero-porosity moduli, E_o and G_o, the porosity dependence constants, b_E and b_G, and Poisson's ratio, ν_o, of 10GCO, NiO-YSZ, and 20GCO samples

Material	*Equation*	E_o	G_o	ν_o	b_E	b_G
10GCO	Exponential	217·81	81·60	0·335	2·92	2·76
	Non-linear	218·08	81·68	0·334	3·01	2·83
	Linear	216·99	81·32	0·334	2·67	2·54
	CSM	218·48	81·94	0·333	1·00	0·88
NiO-YSZ	Exponential	207·13	78·04	0·327	2·48	2·38
	Non-linear	207·22	78·04	0·328	2·55	2·42
	Linear	205·46	77·48	0·326	2·10	2·03
	CSM	218·78	80·58	0·358	0·93	0·77
20GCO	Exponential	213·31	79·91	0·335	2·64	2·47
	Non-linear	213·57	79·98	0·327	2·71	2·52
	Linear	212·24	79·56	0·334	2·39	2·25
	CSM	216·57	81·21	0·333	1·00	0·87

All the equations fitted to the modulus-porosity data from 10 and 20GCO, YSZ, and TZP agree with each other quite well (Figs 2 to 5). Also, the availability of moduli data for very low porosity down to 1·5% yielded very accurate estimation of the zero porosity moduli, as shown for YSZ and TZP in Tables 2 and 3. In the case of equation fitting to the data from NiO-YSZ samples, all the empirical equations agree well with each other. But, the effective moduli, E^* and G^*, calculated by the CSM equations, deviate from those obtained from the empirical equations (Fig. 6). The resulting values of Poisson's ratio are much larger than those calculated from the empirical equations and experimental data. Also, the estimates of E_o and G_o values are about 5% higher than the values from empirical equations (Table 4). The moduli data, corresponding to about 2%

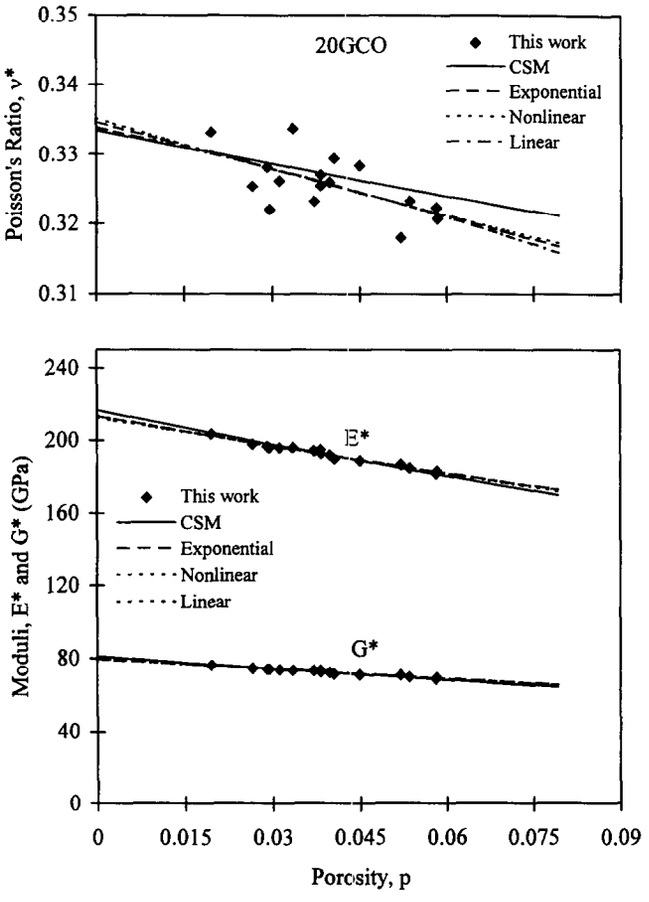

Fig. 5. Effective Young's (E^*) and shear (G^*) moduli and Poisson's ratio (ν^*) as a function of porosity for 20GCO samples. The fitted equations are illustrated by separate lines, as shown in the legend.

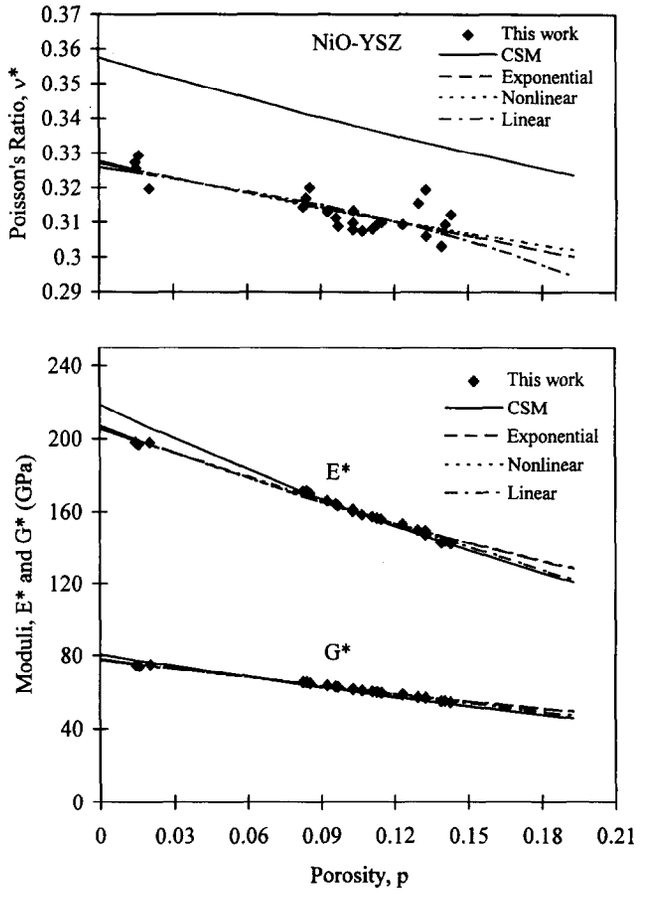

Fig. 6. Effective Young's (E^*) and shear (G^*) moduli and Poisson's ratio (ν^*) as a function of porosity for NiO-YSZ samples. The fitted equations are illustrated by separate lines, as shown in the legend.

Table 5. Goodness of fit of empirical and theoretical (CSM) equations to the experimental modulus-porosity data

Material	*Effective moduli*	*Goodness of fit*, S			
		Exponential	*Non-linear*	*Linear*	*CSM*
10GCO	E^*	0·886	0·886	0·885	0·885
	G^*	0·872	0·872	0·871	0·869
TZP	E^*	0·922	0·920	0·926	0·922
	G^*	0·882	0·881	0·888	0·883
NiO-YSZ	E^*	0·989	0·988	0·995	0·928
	G^*	0·987	0·986	0·994	0·929
20GCO	E^*	0·970	0·970	0·969	0·947
	G^*	0·959	0·959	0·959	0·927
YSZ	E^*	0·990	0·990	0·989	0·975
	G^*	0·982	0·982	0·981	0·963
Average	E^* and G^*	0·944	0·943	0·946	0·923

porosity (Fig. 6), confirm that the CSM equations overestimate the values of E_0 and G_0. It appears that the empirical equations provide a better description of the moduli-porosity relation for the NiO-YSZ samples.

The theoretical model, employed to obtain the moduli-porosity equations of the composite sphere model (CSM), is based on the approximation of a porous structure to an assembly of composite spheres, each formed by a sphere of matrix material with a spherical pore concentrically placed in it.[15,16] The CSM equations (eqns (6) to (8)) were derived on the basis of the following general equation given by Hashin and Shtrikman[12,13]

$$K^* = \frac{\overline{\sigma}_{ij}}{3\overline{e}_{ij}} \qquad (12)$$

where K^* is the effective bulk modulus and $\overline{\sigma}_{ij}$ and $\overline{e}_{ij}$ are volume averages of the hydrostatic stress and strain in the composite sphere, respectively.

The adaptation of eqn (12) to represent the stress and strain distribution in a multi-pore geometry of a two-phase composite structure yields the effective moduli expressions of the CSM theory. In terms of this theoretical model, the composite structure of NiO-YSZ samples contains three phases, including pores, NiO, and YSZ. The inclusion of the third phase, either NiO or YSZ, with different moduli in the composite should result in a change in the volume average of stress and strain, described in eqn (12) in primitive form. Hence, the CSM equations, derived for two-phase composites, may not be valid for estimating the modulus-porosity relations in three-phase composites. This might account for the observed deviation of the CSM moduli and Poisson's ratio of NiO-YSZ from both experimental data and plots of empirical equations at low values of p (Fig. 6).

4.2 Goodness of fit

The goodness of fit parameters, S, of the empirical

Table 6. Percentage standard error in estimating the effective moduli by fitting the empirical and theoretical (CSM) equations to moduli-porosity data

Material	*Moduli*	*Percentage standard error*, $\sigma_{y\cdot x}$			
		Exponential	*Non-linear*	*Linear*	*CSM*
10GCO	E^*	1·30	1·29	1·30	1·34
	G^*	1·17	1·17	1·17	1·23
TZP	E^*	1·43	1·43	1·42	1·45
	G^*	1·70	1·70	1·70	1·73
NiO-YSZ	E^*	0·78	0·77	0·89	0·92
	G^*	0·57	0·56	0·59	0·67
20GCO	E^*	0·98	0·98	0·99	1·12
	G^*	1·08	1·08	1·08	1·25
YSZ	E*	1·01	1·00	1·07	1·12
	G*	1·26	1·24	1·33	1·41
Average of σ for E & G		1·13	1·12	1·15	1·22

and theoretical (CSM) equations to the experimental data (E^* and G^*), determined using eqn (9), are given in Table 5. A second test of the equations against the experimental data was carried out by determining the percentage standard error, σ_{x-y} (eqn (11)) of the E^*, G^* and ν^* of the experimental data sets. The results, presented in Table 6, demonstrate that in all cases the error is less than 2% of the zero porosity values of moduli. Depending on the scatter of the experimental data, the values of S and σ_{x-y} for each equation change from one sample set to another. The values of S for both empirical and CSM equations, fitted to the moduli data from 10 and 20GCO, YSZ, and TZP (Table 5), are very similar and mostly greater than 0·9, indicating very good fit to the experimental data. For these sample sets, there is little to choose between the different equations although the non-linear and exponential equations show slightly better fits.

The empirical equations fitted to the moduli data for NiO-YSZ also yielded similar values of S and σ_{x-y} (Table 6). But the CSM equations gave rise to smaller values of S (about 0·93) and larger percentage standard error than those from the empirical equations. This reflects the possibility that the CSM equations might not hold for calculating the effective moduli of three-phase composites, such as these NiO-YSZ samples.

The difference between the goodness of fits of the different equations is negligibly small in this work. Although these equations fit data equally well over the small range of porosity studied here, further moduli data covering a larger porosity range would be required to determine the accuracy of these equations in estimating the effective moduli of porous solids more generally. Dean and Lopez[8] have tested the empirical equations against a selected set of modulus-porosity data, reported in the literature for different ceramic materials. They found that the linear relation (eqn (3)) gave the best fit. However, the fact that Dean and Lopez[8] fitted the equations to data for a given material produced by different fabrication routes might have masked a small non-linearity observed here.

5 Conclusions

The effective Young's (E^*) and shear (G^*) moduli and Poisson's ratio (ν^*) of some of the materials of interest for solid oxide fuel cells (SOFC), namely 10 and 20% Gd_2O_3-doped CeO_2 (GCO), TZP, YSZ, and NiO-YSZ, were determined at room temperature using the impulse excitation technique on some samples that had been produced in a form compatible with their potential use. The dependence of moduli on porosity was characterized by employing both theoretical (composite sphere method, CSM) and empirical (exponential, non-linear, and linear) equations. The experimental data from our samples showed good agreement with the literature data for YSZ, the only material for which the polycrystalline moduli have been reported previously.

The zero porosity moduli of YSZ and TZP, estimated using the fitted equations, showed good agreement with the previously reported single-crystal moduli of these materials, reinforcing the accuracy of the fitted equations in describing the modulus-porosity relationships. A similar comparison could not be made for 10 and 20GCO due to the lack of single-crystal data. A comparison is not possible in principle for NiO-YSZ since it is a composite material at zero porosity.

The theoretical and empirical equations used were tested by determining the goodness of fit of the equations to the experimental data and the corresponding standard error of estimation. The goodness of fit corresponded to a relative standard deviation of about 1% in estimating the modulus for a given porosity. For 10 and 20GCO, YSZ, and TZP, there was no significant difference between the goodness of fit of all the equations. For NiO-YSZ, the empirical equations were found to yield better fits than the CSM equations. The less good fits obtained for the CSM equations suggest that they are limited in applications to the moduli-porosity relationships in two-phase composites, and are not strictly applicable to materials containing three phases, namely pores, NiO, and YSZ in these materials.

Acknowledgements

The authors gratefully acknowledge the funding provided by the Commission of the European Communities (Contract BRE-CT93-0578), and the supply of samples by ECN Fossil Fuels and DSM of The Netherlands, and Siemens AG Corporate Research and Development of Germany.

References

1. Minh, N.Q., Ceramic fuel cells. *J. Am. Ceram. Soc.*, 1993, **76**(3), 563–588.
2. Ohring, N., *The Materials Science of Thin Films*. Academic Press Inc., Harcourt Brace Jovanovich Publishers, 1991.
3. Scafe, E., Musicanti, S. and Mercuri, S., Young's modulus of thin tape-cast YSZ materials. In *Proceedings of the First European Solid Oxide Fuel Cell Forum*, Vol. 2, ed. U. Bossel. Druckerei J. Kinzel, Germany, 1994, pp. 789–798.

4. Ingel, R. P. and Lewis III, D., Elastic anisotropy in zirconia single crystals. *J. Am. Ceram. Soc,*, 1988, **71**(4), 265–271.
5. Pace, N. G., Saunders, G. A., Sümengen, Z. and Thorp, J. S., The elastic constants and interatomic binding in yttria-stabilised zirconia. *J. Mater. Sci.*, 1969, **4**, 1106-1110.
6. Kandil, H. M., Greiner, J. D. and Smith, J. F., Single-crystal elastic constants of yttria-stabilised zirconia in the range 20° to 700°C. *J. Am. Ceram. Soc.*, 1984, **67**(5), 341–346.
7. Glandus, J. C., Rupture fragile et resistance aux chocs thermiques de ceramiques a usages mechaniques. Ph.D. thesis, University of Limoges, France, 1981, p. 2.13.
8. Dean, E. A. and Lopez, J. A., Empirical dependence of elastic moduli on porosity for ceramic materials. *J. Am. Ceram. Soc.*, 1983, **66**(5), 366–370.
9. Fryexell, R. E. and Chandler, B. A., Creep, strength, expansion, and elastic moduli of sintered BeO as a function of grain size, porosity, and grain orientation. *J. Am. Ceram. Soc.*, 1964, **47**(6), 283–291.
10. Spriggs, R. M., Expression for effect of porosity on elastic modulus of polycrystalline refractory materials, particularly aluminum oxide. *J. Am. Ceram. Soc.*, 1961, **44**, 628–629.
11. Hasselman, D. P. H., On the porosity dependence of the elastic moduli of polycrystalline refractory materials. *J. Am. Ceram. Soc.*, 1962, **54**(9), 452–453.
12. Hashin, Z., Elastic moduli of heterogeneous materials. *J. Appl. Mech.*, 1962, **29**, 143–150.
13. Hashin Z. and Shtrikman, S., A variational approach to the elastic behaviour of multiphase materials. *J. Mech. Phys. Solids*, 1963, **11**(2), 127–140.
14. Budiansky, B., On the elastic moduli of some heterogeneous materials. *J. Mech. Phys. Solids*, 1965, **13**(4), 223–227.
15. Ramakrishnan, N. and Arunachalam, V. S., Effective elastic moduli of porous solids. *J. Mater. Sci.*, 1990, **25**, 3930–3937.
16. Ramakrishnan, N. and Arunachalam, V. S., Effective elastic moduli of porous ceramic materials. *J. Am. Ceram. Soc.*, 1993, **76**(11), 2745–2752.
17. Love, A. E. H., *A Treatise on the Mathematical Theory of Elasticity*, 4th edn. Dover Publications, New York, 1944.
18. Winnubst, A. J. A., Keizer, K. and Burggraaf, A. J., Mechanical properties and fracture behaviour of ZrO_2–Y_2O_3 ceramics. *J. Mater. Sci.*, 1983, **18**, 1958–1966.
19. Buckley, J. D. and Braski, D. N., Elastic modulus of stabilised zirconia. *J. Am. Ceram. Soc.*, 1967, **50**(4), 220–221.
20. Sammes N. M. and Zhang Y., High temperature mechanical properties of $(CeO_2)_{1-x}(Gd_2O_3)_x$ electrolytes. In *Second European Solid Oxide Fuel Cell Forum*, 6–10 May 1996, Norway, Vol. 2, pp. 697–706.